frontiers | Frontiers in Earth Science

TYPE Original Research
PUBLISHED 18 September 2024
DOI 10.3389/feart.2024.1439493

OPEN ACCESS

EDITED BY
Giovanni Martinelli,
National Institute of Geophysics and Volcanology, Section of Palermo, Italy

REVIEWED BY
Jia Cheng,
China University of Geosciences, China
Xiaocheng Zhou,
China Earthquake Administration, China
Mita Uthaman,
Indian Institute of Technology Kharagpur, India
Arnab Roy,
University of Idaho, United States

*CORRESPONDENCE
Junshan Xu,
junshanxu@ninhm.ac.cn
Xiangfang Zeng,
zengxf@whigg.ac.cn

RECEIVED 28 May 2024
ACCEPTED 03 September 2024
PUBLISHED 18 September 2024

CITATION
Xu J and Zeng X (2024) Stress modeling for the upper and lower crust along the Anninghe, Xianshuihe, and Longmenshan Faults in southeastern Tibetan plateau. *Front. Earth Sci.* 12:1439493. doi: 10.3389/feart.2024.1439493

Stress modeling for the upper and lower crust along the Anninghe, Xianshuihe, and Longmenshan Faults in southeastern Tibetan plateau

Junshan Xu[1]* and Xiangfang Zeng[2]*

[1]Key Laboratory of Crustal Dynamics, National Institute of Natural Hazards, Ministry of Emergency Management of China, Beijing, China, [2]State Key Laboratory of Geodesy and Earth's Dynamics, Innovation Academy for Precision Measurement Science and Technology, Chinese Academy of Sciences, Wuhan, China

Earthquake occurrence depth in the crust is related to stress, temperature, and brittle–ductile transition, which is also near the transition depth of the upper to lower crust. The composition variation between the upper and lower crust causes remarkable changes of rheological properties and variation in stress distribution. Clarifying the detailed stress distribution in the upper and lower crust is crucial for understanding the brittle–ductile transition and the stress environment of the seismogenic zone. The Southeastern Tibetan Plateau (SETP), with wide spread of active strike–slip faults and clustered earthquakes, provides a natural field for investigating the relationships between crustal stresses, deformation behaviors, and earthquake mechanics. By considering the rheological properties of granite and anorthite, this paper established stress models with different boundary depths (15, 20 and 25 km) between the upper and lower crust along the Anninghe, Xianshuihe, and Longmenshan Faults in the SETP with a horizontal strain of 6×10^{-4} extracted from *in situ* stress data. The stress model with different geothermal gradients and a boundary depth of 20 km between the upper and lower crust suggests two distinct types of the brittle–ductile transition below these three faults. Simultaneously, the stress model can account for the continuity of earthquake depth distribution below the Longmenshan Fault and the seismic gap below the Anninghe and Xianshuihe Faults. The continuity of earthquake depth distribution or seismic gap below these three faults can be explained by their different geothermal gradients. These findings provide new insights for understanding the stress environment of the seismogenic zone in the SETP. Our model reveals the relationships between differential stress, seismicity, brittle–ductile transition, and boundary depth of the upper and lower crust in the continental crust, and connects the multiple observations from geophysics and geology. Furthermore, our model provides insights for studying multiple processes in the continental crust, such as crustal deformation, fault slip, and earthquake occurring.

KEYWORDS

brittle-ductile transition, stress modeling, earthquake depth, Anninghe Fault, Xianshuihe Fault, Longmenshan Fault

1 Introduction

Brittle–ductile transition in the crust is related to not only the change of deformation behaviors due to temperature increase but also the variations of stress, seismicity, and even the transition from the upper to lower crust (Maggi et al., 2000; Jackson, 2002; Scholz, 2002; Bürgmann and Dresen, 2008). Usually, the boundary of the upper to lower crust (denoted as UL boundary hereinafter) corresponds to the compositional decrease in SiO_2 content from 67 wt% to less than 64 wt% (Rudnick and Gao, 2003; Hacker et al., 2015), which suggests the increase in feldspars and pyroxenes and the change of stress sustainability (Bürgmann and Dresen, 2008; Xu and Zeng, 2022) due to the substantially different rheological properties of rocks or minerals (Gleason and Tullis, 1995; Rybacki and Dresen, 2000; Chen et al., 2021; Fukuda et al., 2022; Masuti et al., 2023). Therefore, determining the UL boundary is crucial to understanding the stress distribution in the crust (related to brittle–ductile transition) and the stress environment of the seismogenic zone (related to earthquake depth). The southeastern Tibetan Plateau (SETP) is the eastward extrusion zone of the India–Asia collision, exhibiting strong tectonic movement and continuous crustal deformation (Li et al., 2019; Wang and Shen, 2020). Active strike–slip faults (such as the Xianshuihe, Anninghe, and Longmenshan Faults, Figure 1) with clustered earthquakes provide a natural field for investigating the relationships between crustal stress, brittle–ductile transition, and earthquake depth (Royden et al., 1997; Royden et al., 2008; Clark and Royden, 2000; An et al., 2001; Tapponnier et al., 2001; Meade, 2007; Huang et al., 2009; Zhang, 2008).

Detailed distribution of crustal stress at different depths can directly reflect the behaviors of the deformation and mechanics of the earthquake (Scholz, 2002); however, only the stress variation (stress drop) before and after the earthquake can be obtained by seismic methods. Stresses in the deep crust are mainly controlled by three aspects (Zang and Stephansson, 2010): (1) gravity, which causes vertical stress; (2) horizontal tectonic strain, which causes horizontal stress; (3) rheological deformation and fault friction strength, which diminish and constrain differential stress. Vertical stress is easy to obtain based on overburden rocks. Horizontal tectonic stress can mostly be acquired through analyzing and extrapolating *in situ* stress data measured at shallow depth because conducting stress measurement at depth larger than 1 km is extremely difficult. Until now, conducting stress measurements is nearly impossible at the depth (> 10 km) of the seismogenic zone where stress magnitude may be hundreds of megapascals (Hanks and Raleigh, 1980; Zang and Stephansson, 2010). The *in situ* stress data used in this study were only conducted within 1 km depth, and they are currently the deepest measurement data in the SETP. Directly extrapolating the measured stress at shallow depth into deep depth usually causes large errors because analyzing the stress data needs to exclude the effects from multiple factors such as topography and geologic structure (Brown and Hoek, 1978; Haimson, 1978; Zoback, 1992; Sheorey, 1994; Fairhurst, 2003; Sen and Sadagah, 2002; Zang and Stephansson, 2010; Heidbach et al., 2019). Hence, in this paper, a method was developed through extracting the horizontal strain from measured stress data to calculate the stress at deep depth. The elastic strain caused by horizontal deformation can be assumed constant in the whole elastic crust (Blanton and Olson, 1999). The present *in situ* stress data contain the information of the elastic strain in elastic crust because they are mainly due to the tectonic horizontal deformation. Therefore, the extracted horizontal elastic strain from *in situ* stress data at shallow depth can be used to calculate stresses at deep depth. Furthermore, the effects of rheological deformation on differential stress is controlled by rock rheological properties and temperature. The geothermal gradients for each fault and the UL boundary depth (related to rock composition variation) also need to be considered. Thus, all the stress components (such as horizontal stress, differential stress, and shear and normal stress in a fault plane) at different depths can be obtained. Stresses on fault and slip possibility of fault can also be discussed.

In this study, we analyzed *in situ* stress data measured in five boreholes in the SETP (Figure 1), extracted the corresponding tectonic strain based on the biaxial stress model (Savage et al., 1992), and calculated stresses for both the upper and lower crust along the strike of fault planes by considering the composition change between the upper and lower crust and the rheological properties of rocks. Results suggest that stress distribution for the upper and lower crust with a UL boundary depth of 20 km in the SETP and different geothermal gradients can account for the geophysical, geological, and laboratory observations (such as the earthquake depth distribution, velocity structures, electrical conductivity structures, geothermal gradient, SiO_2 content, and rock rheological properties).

2 Methods

2.1 Overview of methods

First, the maximum horizontal strain of tectonic deformation was extracted from *in situ* stress data. Second, based on the obtained horizontal strain, the horizontal, vertical, and differential stresses for the upper and lower crust were calculated by considering the constrains of rock rheological properties and geothermal gradients along three faults (Anninghe, Xianshuihe, and Longmenshan Faults). Third, the ratio of shear stress to normal stress, which is useful for analyzing the occurring of earthquake and slip, was obtained. Finally, the detailed distribution of differential stress and ratio of shear stress to normal stress along each fault at different depths in the upper and lower crust were determined.

2.2 Extraction of maximum horizontal strain ε_H

In this study, the stresses in the deep crust were calculated using a method based on the horizontal strain, which is extracted from the *in situ* stress data measured in boreholes. The relationship between horizontal strains and stresses was calculated using Equation 1 (Savage et al., 1992; Sheorey, 1994):

$$\begin{aligned} S_H &= \frac{E}{1-\nu^2}\left(\varepsilon_H + \nu\varepsilon_h\right) + \frac{\nu}{1-\nu}S_V \\ S_h &= \frac{E}{1-\nu^2}\left(\varepsilon_h + \nu\varepsilon_H\right) + \frac{\nu}{1-\nu}S_V \end{aligned} \tag{1}$$

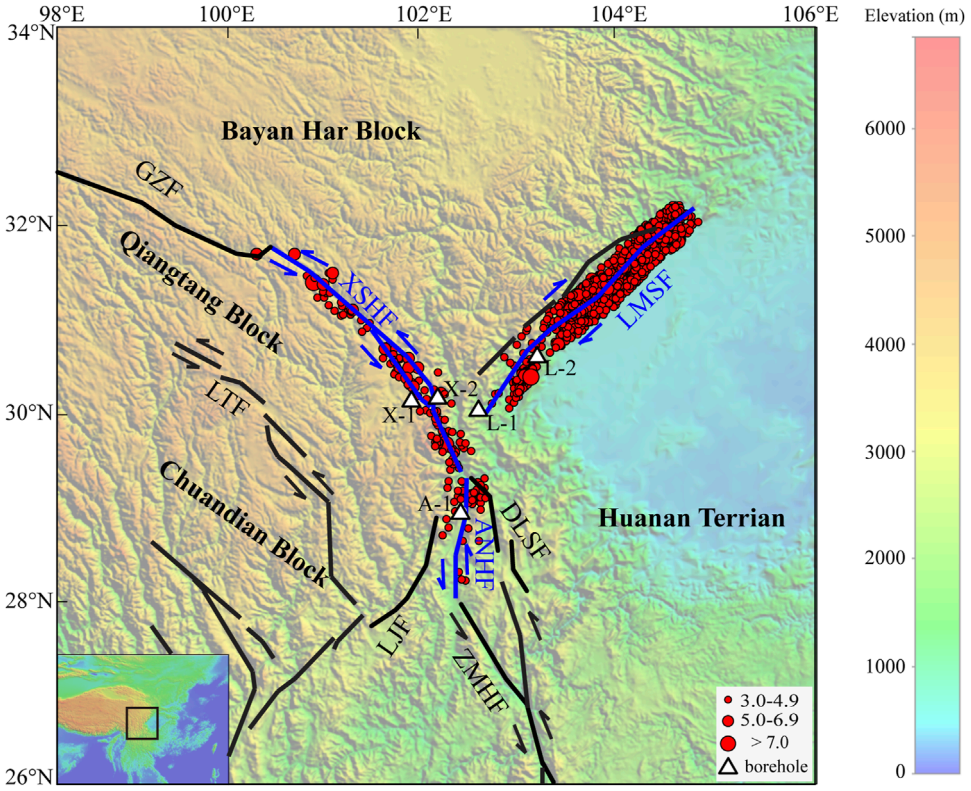

FIGURE 1
Tectonic map and borehole locations. Purple triangles indicate the locations of *in situ* stress measurement boreholes and purple characters are their names. The blue solid lines indicate the faults of Anninghe (ANHF), Xianshuihe (XSHF), and Longmenshan (LMSF). The black solid lines indicate the following faults: LTF, Litang Fault; GZF, Ganzi Fault; LJF, Lijiang Fault; DLSF, Dalianshan Fault; and ZMHF, Zemuhe Fault. Events with $Ms \geq 3.0$ within a distance of 20 km along ANHF, XSHF, and LMSF in the period 1971.1–2022.3 are used (also in the following figures), which are download from China National Seismic Data Center (https://data.earthquake.cn/gcywfl/index.html).

where S_H and S_h are the maximum and minimum horizontal stresses, respectively; ε_H and ε_h are the maximum and minimum horizontal strains, respectively; ν is the Poisson's ratio; E is the Young's modulus; and S_V is the vertical stress. Given that the SETP is located in the strong and continuous crustal deformation area of the India–Asia collision zone (Li et al., 2019; Wang and Shen, 2020), the relationship between ε_H and ε_h is supposed to obey a simple compressive form $\varepsilon_h = \nu\varepsilon_H$ and ε_H is supposed to be vertically uniform in the elastic crust (Blanton and Olson, 1999). Thus, the magnitude of horizontal stresses S_H and S_h can be calculated using Equation 2:

$$\begin{aligned} S_H &= \frac{1+\nu^2}{1-\nu^2}E\varepsilon_H + \frac{\nu}{1-\nu}S_V \\ S_h &= \frac{2\nu}{1-\nu^2}E\varepsilon_H + \frac{\nu}{1-\nu}S_V \end{aligned} \tag{2}$$

S_H and S_h values were obtained within a depth range of 300–1,400 m by hydraulic fracturing method from five boreholes located in the SETP as shown in Figure 1 (Ren et al., 2021; Li et al., 2022). All stress data were measured from granite, whose mechanical parameters (E and ν) usually exhibit a similar trend at the effective pressure range of 5–30 MPa (Nur and Simons, 1969; Blake et al., 2019). S_V can be estimated based on the lithostatic state with a density of 2.65 g/cm^3 (Ren et al., 2021). Therefore, ε_H can be calculated using Equation 2.

2.3 Calculation of horizontal stresses S_H and S_h and differential stress σ_D

From the extracted value of ε_H, the values of S_H and S_h in different depths were calculated using Equation 2. Then differential stress σ_D was calculated according to the difference between S_H–S_h in the shallow depth (S_H>S_V) and S_V–S_h in the deep part (S_V>S_H). Simultaneously, in the deep crust, σ_D is also constrained by the rock creep due to high temperatures, obeying the power law equation shown as Equation 3.

$$\frac{d\varepsilon_v}{dt} = A{\sigma_D}^n \exp\left(-\frac{Q}{RT}\right) \tag{3}$$

where $\frac{d\varepsilon_v}{dt}$ is the viscous strain rate, A is a constant, σ_D is the differential stress, n is the stress exponent, Q is the activation energy, R is the molar gas constant, and T is the absolute temperature. The temperatures at different depths were calculated based on the geothermal gradient obtained by Wang et al. (2018), in which they first estimated the Curie-point depths using the centroid spectral approach based on 3D fractal magnetization model (Tanaka et al., 1999; Li et al., 2017) and then calculated the crustal temperature structures using 1D steady thermal conduction equation. In accordance with previous studies (Wang and Shen, 2020; Sun et al., 2021), a strain rate of 1×10^{-14} s^{-1} was used as

the brittle–ductile transition boundary. Granite (we use the data of granitoid in Rutter et al. (2006), which is consistent with the composition of the upper crust, ~67% SiO_2 content) was taken as the composition of the upper crust, and 80% granite–20% anorthite (~64% SiO_2 content) was set for the lower crust to accommodate the compositional transition from the upper to the lower crust that corresponds to the decrease in SiO_2 content from 67 wt% to no more than 64 wt% due to the increase in feldspars and pyroxenes (e.g., Hacker et al., 2015). Three different depths of UL boundary, namely, 15, 20, and 25 km, were considered to analyze the stress distribution in the upper and lower crust. The rheological parameter of granite is as follows: A is $10^{-12.2}$ s^{-1}, n is 1.8, and Q is 220 *kJ/mol* (Rutter et al., 2006). For anorthite, A is $10^{-12.7}$ s^{-1}, n is 3.0, and Q is 648 *kJ/mol* (Rybacki and Dresen, 2000). For the composition of 80% granite–20% anorthite, A is $10^{-12.3}$ s^{-1}, n is 2.0, and Q is 289 *kJ/mol* according to the multiphase flow law shown as Equation 4 (Tullis et al., 1991; Ji and Zhao, 1993).

$$\begin{cases} n = 10^{(f_1 \log n_1 + f_2 \log n_2)} \\ Q = \dfrac{Q_2(n-n_1) - Q_1(n-n_2)}{n_2 - n_1} \\ A = 10^{[\log A_2(n-n_1) - \log A_2(n-n_2)]} \end{cases} \quad (4)$$

where f_1 = 0.8 and f_2 = 0.2 are the compositional ratios of granite and anorthite, respectively. Q_1, Q_2, n_1, n_2, A_1, and A_2 are the corresponding parameters of power law equations for granite and anorthite, respectively.

2.4 Calculation of the ratio of shear stress to normal stress (τ/σ_n)

According to the Coulomb–Mohr criterion ($\tau = \mu\sigma_n + cohn$, where τ is the shear stress, μ is the static friction coefficient, σ_n is the normal stress on the fault plane, and *cohn* is the cohesion), the τ/σ_n ratio can be roughly taken as the potential friction coefficient μ because the cohesive strength of a fault is relatively unimportant compared with the stress magnitude at deep depth (Zoback et al., 2003; Zang and Stephansson, 2010). Usually, the measured value of S_H is larger than that of S_V at very shallow depth, and S_V becomes larger than S_H with increasing depth (Sheorey, 1994; Yang et al., 2012). Therefore, with S_H, S_h, and S_V as the three principal stresses, they correspond to σ_1, σ_2, and σ_3 in the shallow depth, respectively, and σ_2, σ_3, and σ_1 in the deep part, respectively. The τ and σ_n on the fault plane were the calculated according to the angle of plane strike and dip. The strikes for the Anninghe, Xianshuihe, and Longmenshan Faults are 0°, 130°, and 45°, respectively (Xu et al., 2003). The dip angles for all of them were set to be 90°. The principal stress was set to be NW30° for the Anninghe Fault and E–W for the Xianshuihe and Longmenshan Faults according to the *in situ* stress measurement and focal mechanism results (Chen et al., 2012; Yang et al., 2021). For the part in the deep crust where the rheological deformation rate is higher than 10^{-14} s, τ/σ_n was set to be 1.0, indicating that the friction strength cannot sustain the value of τ and fault slip may occur. Pore pressure P_0, a critical parameter for slip in the actual crust, was also considered and set to be equal to the hydrostatic pressure (Hubbert and Rubey, 1959; Zoback and Townend, 2001).

3 Results

Figure 2 shows the results of calculated and measured maximum horizontal stresses S_H for the five boreholes. The obtained maximum horizontal strain ε_H for borehole A-1 (located in the Anninghe Fault area) is 3–6 × 10^{-4}; those for X-1 and X-2 (located in the Xianshuihe Fault area) are 4–6 × 10^{-4} and 6–6.5 × 10^{-4}, respectively, and those for L-1 and L-2 (located in the Longmenshan Fault area) are both 5–7 × 10^{-4}. Although the measured stress shows variation at the very shallow depth, the ε_H in the relatively deep (>900 m) part of these boreholes is close to 6 × 10^{-4} (Chen et al., 2012; Ren et al., 2021; Li et al., 2022). The minimal difference in ε_H among the different boreholes suggests that the accumulated strain in the SETP is similar. This finding demonstrates that horizontal strain is a suitable parameter to describe the magnitude of deformation caused by tectonic movement.

The distributions of calculated differential stress σ_D with different depths of UL boundary and focal depth along the Anninghe, Xianshuihe, and Longmenshan Faults are shown in Figure 3, Supplementary Figures S1, S2 (in Supplementary Materials). A low-stress layer can be generated at the bottom of granite layer for all of the three faults with a UL boundary depth of 25 km (Supplementary Figure S1, in Supplementary Materials) but not for all of them with a UL boundary depth of 15 km (Supplementary Figure S2, in Supplementary Materials). When the UL boundary depth is 20 km, a clear low-stress layer is generated below the Anninghe and Xianshuihe Faults, yet it is nearly absent beneath the Longmenshan Fault (Figure 3). The distribution of seismic events demonstrates inconsistency with the stress distribution predicted at a boundary depth of 25 km, where many earthquakes occur in the low-stress layer.

The distributions of τ/σ_n ratio along the three faults are shown in Figure 4 Supplementary Figures S3, S4 (in Supplementary Materials). τ/σ_n exhibits an increasing trend with the depth, and most earthquakes are located in a domain with τ/σ_n of 0.5–0.8 (Figure 4). This finding can be explained by Byerlee's law Byerlee (1978), which states that a slip condition occurs when the friction coefficient μ reaches a critical value of 0.6–0.85. The Byerlee's law describes the friction strength of rocks when brittle deformation is dominant at proper temperatures. The composition of 80% granite–20% anorthite has higher strength than pure granite, and exhibits brittle deformation at higher temperatures. Therefore, the Byerlee's law works in the layer of 80% granite–20% anorthite at a deep depth. In addition, the vertical statistical distributions of focal depth for the Anninghe and Xianshuihe Faults show a decrease at 16–20 km (seismic gap in Figure 5) and an increase below 20 km, especially for magnitude Ms≥4.0. No similar phenomenon is observed for the Longmenshan Fault (Figure 5). The numbers of earthquakes with magnitude Ms≥4.0 below all the three faults tend to zero at a depth larger than 22 km, which may be caused by the low differential stress or high ratio of τ/σ_n. These phenomena are analogous to the corresponding distribution of differential stress against depth for the results with a UL boundary depth of 20 km instead of 15 km. Thus, the decreased number of seismic events at 16–20 km depth below the Anninghe and Xianshuihe Faults can be explained by the low differential stress due to granite rheological behavior. The increased number at 20 km depth and the near

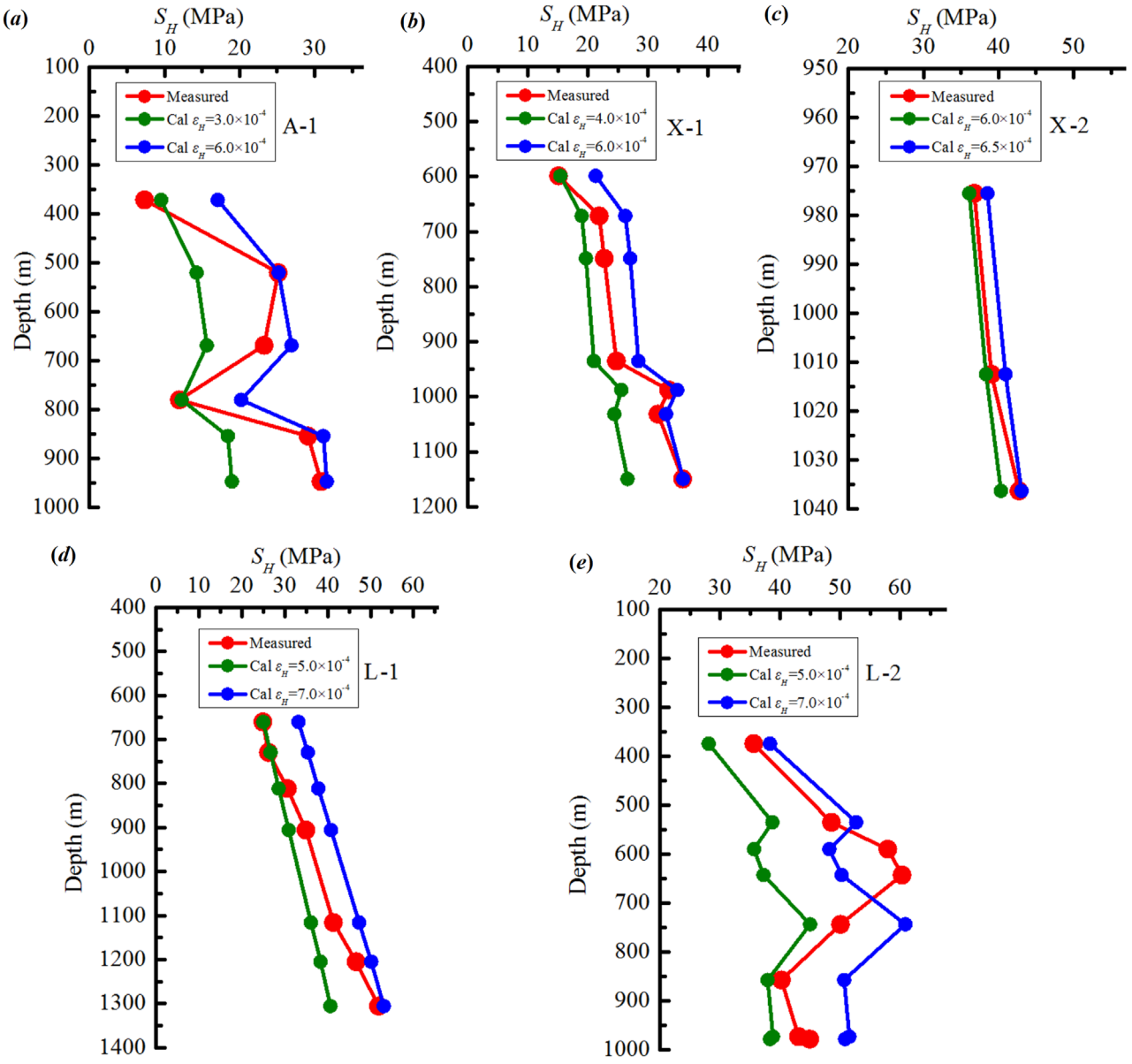

FIGURE 2
Measured and calculated data of the *in situ* stress of S_H. Measured and calculated data of S_H in boreholes A-1 **(A)**, X-1 **(B)**, X-2 **(C)**, L-1 **(D)**, and L-2 **(E)**. The measured stress data for borehole X-1, X-2 and L-1 are from Ren et al. (2021). Those for borehole L-2 and A-1 are from Li et al. (2022) and the present study, respectively.

disappearance at below 22 km are attributed to the existence of the layer of 80% granite–20% anorthite. The granite rheological layer below the Longmenshan Fault is not evident. This phenomenon is probably due to its relatively lower geothermal gradient (~17°C/km) than the Anninghe (~21°C/km) and Xianshuihe (~19°C/km) Faults, which are obtained by averaging the results of Wang et al. (2018) along these three faults. The relatively high geothermal gradient in the Anninghe and Xianshuihe Faults compared with that of the Longmenshan Fault is also demonstrated by observations of geothermal water (Tian et al., 2021). The geothermal gradient results in Wang et al. (2018) cannot exhibit local details because of low resolution but provide larger scale results within the SETP. The local measured geothermal gradients may differ from our data or change largely even along the same fault (e.g., Liu et al., 2017; Cheng et al., 2022; Ullah et al., 2022).

The decrease in differential stress below or above 20 km corresponds to the brittle–ductile transition. The depth of the brittle–ductile transition is similar to the depth of the UL boundary but is also influenced by the UL boundary because the anorthite in the lower crust increases the sustainability of differential stress. Therefore, the brittle–ductile transition can cause low seismicity due to dissipated differential stress, whereas the transition between the upper to lower crust may increase seismicity due to increased differential stress.

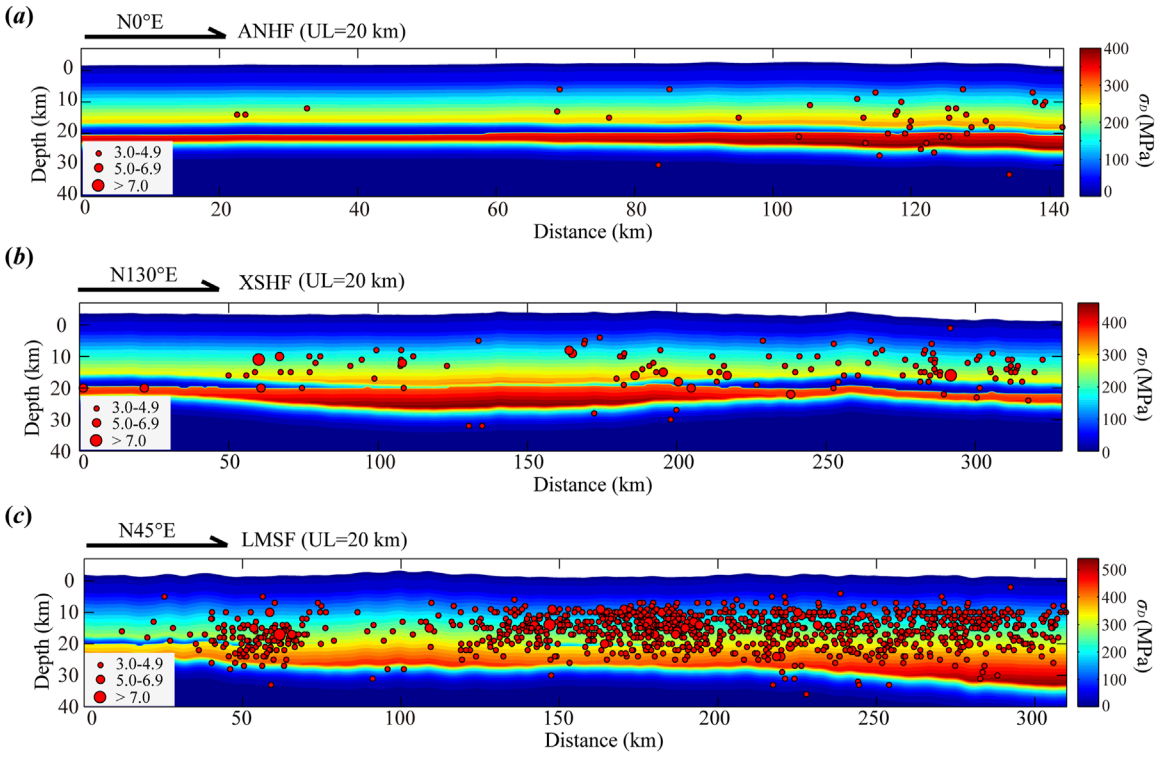

FIGURE 3
Distribution of differential stress (σ_D) and the focal depth along the faults with a UL boundary depth of 20 km (UL = 20 km). **(A)** Anninghe Fault (ANHF), **(B)** Xianshuihe Fault (XSHF), and **(C)** Longmenshan Fault (LMSF).

4 Discussion

4.1 UL boundary, brittle–ductile transition, and differential stress in the SETP

The consistency between our stress model and the vertical distribution of focal depth suggests that the depth of the UL boundary in the SETP is approximately 20 km (Figure 3). In particular, the low-stress layers at depth 16–20 km along the XSHF and ANHF have few seismic events. Most seismic events are located in high stress areas, which are below, above, and around these low-stress areas. In consideration of the 5 km average height of India–Asia collision, the 20 km depth of the upper crust is also comparable with the model of CRUST1.0, which shows a 26.2 km thickness of the upper crust for the India–Asia collision zone (Laske et al., 2013; Hacker et al., 2015). Our stress model in the deep part is essentially sensitive to geothermal gradient, which is extracted from the magnetic anomalies (Wang et al., 2018) and also verified by the measured results in boreholes LMS-2 (15°C/km, Li et al., 2022) and ANH (24°C/km, measured in this study). Errors of focal depths, which may reach to 5 km even after relocation (Liu et al., 2023), influence the judgment of UL boundary. Therefore, earthquakes Ms < 3.0 were excluded in this study. The low-stress layer in our model at a depth range of 16–20 km below the Anninghe and Xianshuihe Faults probably corresponds to low electrical conductivity as observed by magnetotelluric imaging (Zhao et al., 2008) and a decrease in velocity structures (Wang et al., 2007). At a depth below 16 km, the low strength of granite can be deformed easily, supporting the possible crustal channel flow suggested by the low electrical conductivity (Zhao et al., 2008; Wan et al., 2010) and tomography (Bao et al., 2015). The velocity structures below the Xianshuihe Fault show a decreased value from 6.10 km/s to 5.85 km/s at the depth of approximately 16 km but without a decrease below the Longmenshan Fault (Wang et al., 2007). The increase in velocity (from 5.85 km/s to 6.25 km/s) at a depth of approximately 20 km is probably caused by the increased content of pyroxenes or feldspars (e.g., anorthite in our model), which can sustain a larger differential stress under a relatively higher temperature than granite. Though constrained by the resolution, the velocity structures along the three faults (Supplementary Figures S5, S6, in Supplementary Materials) interpolated from the high-resolution community velocity model V2.0 of southwest China (Liu et al., 2023) also suggest that the low-velocity layers are identifiable below the Anninghe and Xianshuihe Faults but almost disappear below the Longmenshan Fault.

The low-stress layer in our model below the Anninghe Fault suggests a different type of brittle–ductile transition from that below the Longmenshan Fault, whereas both types partially exist below the Xianshuihe Fault. Figure 6 shows schematic plots of differential stress against depth. In Figure 6A, the brittle–ductile transition can be generated in the granite and 80% granite–20% anorthite layers (Type A: double-layer brittle–ductile transition), whereas in Figure 6B, it only appears in the 80% granite–20%

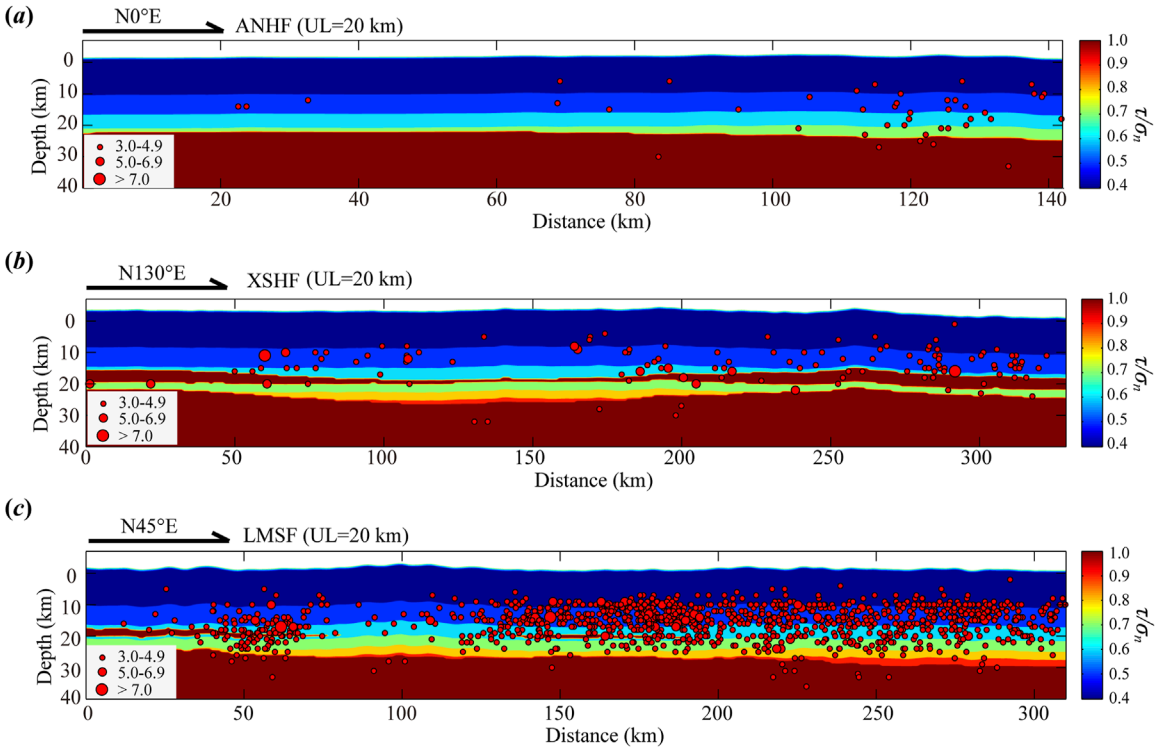

FIGURE 4
Distribution of the ratio between shear and normal stresses (τ/σ_n) and the focal depth along the faults with a UL boundary depth of 20 km (UL = 20 km). **(A)** Anninghe Fault (ANHF), **(B)** Xianshuihe Fault (XSHF), **(C)** Longmenshan Fault (LMSF).

anorthite layer (Type B: single-layer brittle–ductile transition). Here in the SETP as part of India–Asia collision zone, the crustal thickness of the crust is in a range of 55–60 km (Hu et al., 2011; Wang et al., 2017); therefore, the depth of the UL boundary can also influence the brittle–ductile transition. Comparing the stress results between Figure 3 and Supplementary Figure S1 reveals that if the depth of the UL boundary changes from 20 km to 15 km, the brittle–ductile transition below the Anninghe and Xianshuihe Faults can switch from Type A to Type B. The decrease in differential stress corresponds to the brittle–ductile transition and causes the decrease of seismicity (Figure 3). However, the seismicity decrease is not totally caused by the brittle–ductile transition in the deep crust because a high τ/σ_n ratio may facilitate fault slip (or free slip) without seismicity. This outcome is verified by comparing Figures 3, 4, where the locations with highest differential stress at around 25 km depth and high τ/σ_n ratio exhibit low seismicity. The brittle–ductile transition is essentially the reduction in differential stress, different from the transition between the upper and lower crust. The composition variations in the transition between upper and lower crust influence the differential stress, thereby the styles of brittle–ductile transition (Rudnick and Gao, 2003; Bürgmann and Dresen, 2008; Hacker et al., 2015). Furthermore, the brittle–ductile transition is complex because the experimental results of rock deformation suggest this transition is generally affected by deformation mechanism, water content, and even grain size of rocks (Zhou et al., 2017; Chen et al., 2021; Fukuda et al., 2022; Masuti et al., 2023).

Differential stress is a basis of the maximum shear stress and associated with the stress drop of earthquake (Aki and Richards, 1980). The stress values in our model shown in Figure 3 Supplementary Figures S1, S2 mainly exhibit a potential stress possibility, indicating the ability of rocks to withstand differential stress. The true values of stress is locally sensitive to many factors, such as the angle between fault strike and principal stress and pore pressure. The differential stress in the deep crust depends on the strength of rocks and the friction strength of faults, which is controlled by the intrinsic frictional strength of faulted rock and the pore pressure at different depths (Hubbert and Rubey, 1959). Therefore, the differential stress in the part with τ/σ_n ratio smaller than 0.6 (mainly in the upper crust) can be sustained with no slip occurring, exhibiting the elastic properties constrained by tectonic movement. The differential stress in the part with τ/σ_n ratio larger than 0.6 (mainly in the lower crust) suggests that the friction property plays an important role. The τ/σ_n ratio decreases with the increasing strain and is also affected by the angle between strike and maximum stress direction. If slip occurs, then the actual stress magnitude in the lower crust is no more than that of the upper crust. Whether pore pressure can develop in the lower crust remains controversial. Observations from deep boreholes at several locations worldwide indicate that hydrostatic pore pressures persist to depths as deep as 12 km in the upper crust (Zoback and Townend, 2001). The stress value in the lower crust with a composition of 80% granite–20% anorthite is consistent with that

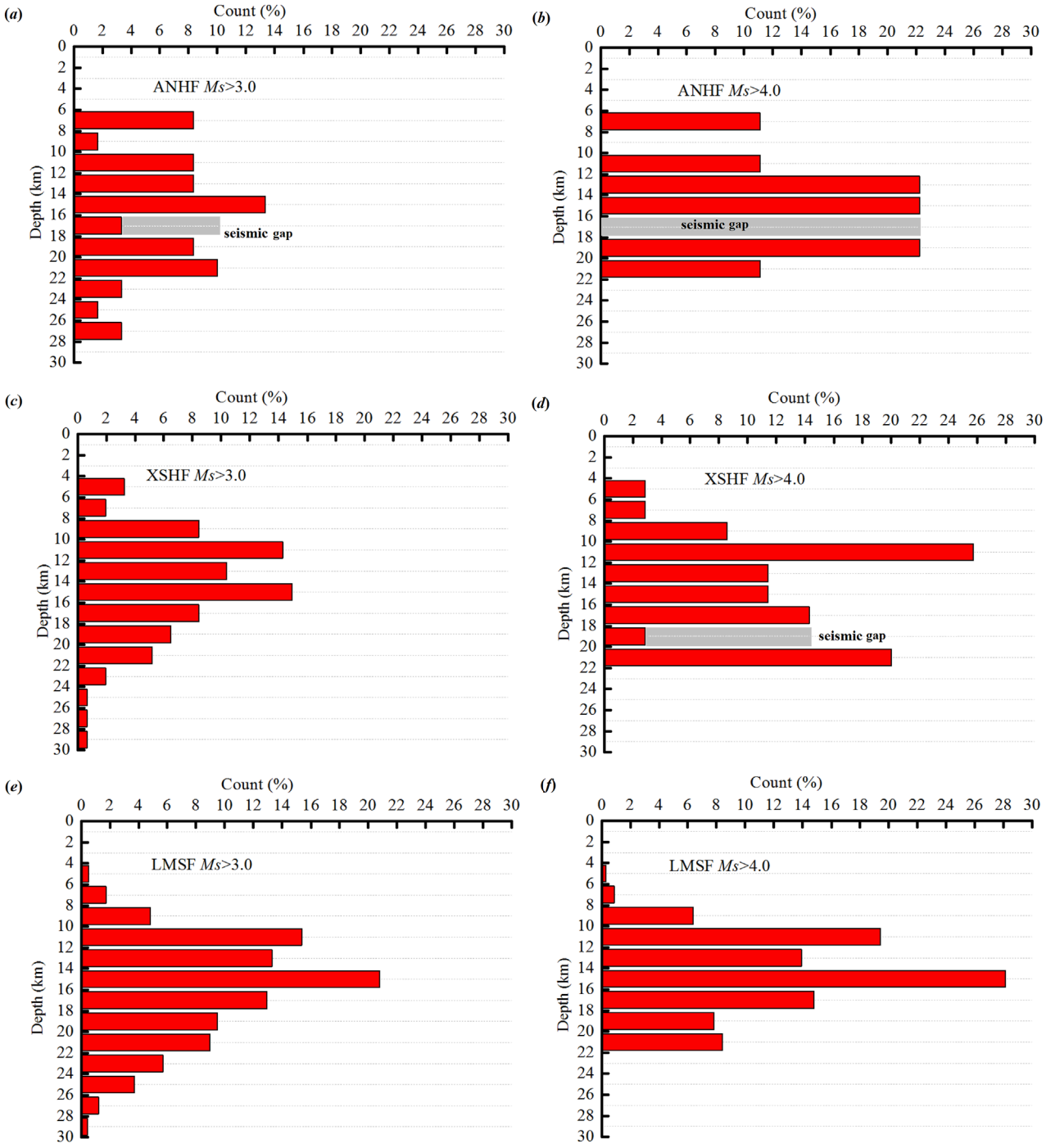

FIGURE 5
Statistical focal distribution against depth. Statistical focal distribution of seismic events in ANHF $M_S \geq 3.0$ **(A)** and $M_S \geq 4.0$ **(B)**, XSHF $M_S \geq 3.0$ **(C)** and $M_S \geq 4.0$ **(D)**, and LMSF $M_S \geq 3.0$ **(E)** and $M_S \geq 4.0$ **(F)**. The earthquake distribution against depth with an interval of 2 km along the three faults were analyzed and compared with the stress distribution. The events with $Ms \geq 3.0$ and $Ms \geq 4.0$ away from the fault plane within 20 km were used. All the events were from the period 1971.1–2022.3 and the China National Seismic Data Center with a website: https://data.earthquake.cn/gcywfl/index.html.

in the lower crust with SiO_2 content of no more than 64 wt% (Hacker et al., 2015). If the bottom of the lower crust has 53 wt% SiO_2 content (Hacker et al., 2015), then the corresponding group with composition of granite50%–anorthite50% sustains larger differential stress in deeper depths than that of 80% granite–20% anorthite. Different compositions in the lower crust may influence the stress magnitude according to the flow equations (Bürgmann and Dresen, 2008). The increase in feldspar and pyroxene promotes stress and strength in the lower crust, providing shear stress for seismogenic processes.

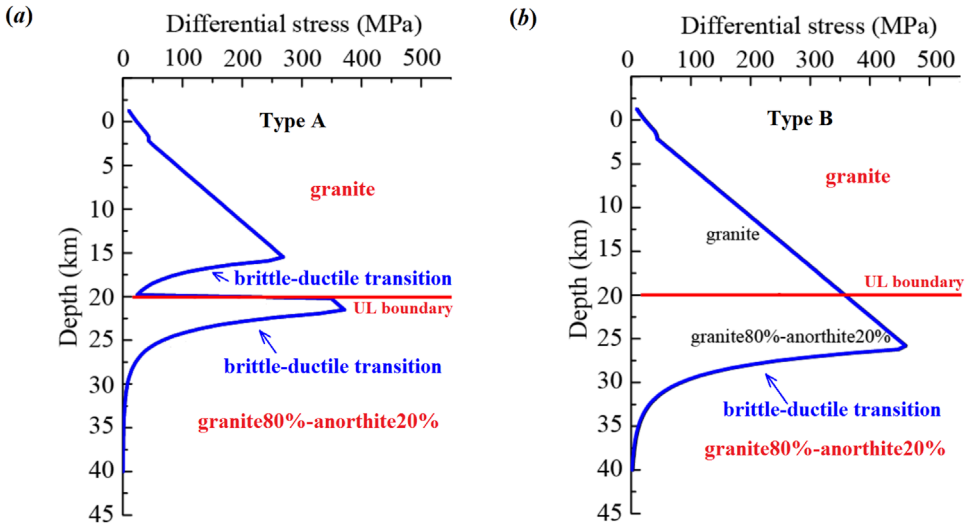

FIGURE 6
Schematic plots of differential stress against depth. **(A)** Typical curve of differential stress below the Anninghe Fault with a 20 km depth of the UL boundary. **(B)** Typical curve of differential stress below the Longmenshan Fault with a 20 km depth of the UL boundary.

It is pointed out that the calculation of differential stress constrained by rock creep is concentrated on in this study, and the plastic strength of faults and rocks was not considered. Actually, the areas with a high τ/σ_n ratio suggest the possible locations for plastic deformation caused by slip of faults or fracture of rocks, and the plastic deformation impacts the overall strength calculations through diminishing differential stress in a more transient way compared with rock creep. In addition, our model provides the stress estimation in the deep crust in accordance with the current absolute strain revealed by *in situ* stress data, and the variation in strain within a short term cannot be detected by the resolution of stress measurements. The calculated differential stress constrained by the strain rate of the rock creep equation reveals the upper limits of differential stress because the deviatoric strain rate was also not considered in this study.

4.2 Strain–stress accumulation and seismic activity

The maximum horizontal strain ε_H indicates the local accumulation of absolute strain caused by tectonic movement, providing the basic stress accumulation for seismogenic processes. Although the Anninghe and Xianshuihe Faults are a lateral strike slip fault and the Longmenshan Fault mainly shows compression shortening (Wang et al., 2008; Zhang, 2008), the similar strain magnitude for these three faults suggests that the local strain is in a relatively stable and balanced state in the SETP. The derived horizontal strain is assumed constant at different depth in the elastic crust in this study, and the values of strain are obtained based on stress data from 1 km depth borehole. It is still possible that the horizontal strain increases with depth. However, the increment may not be larger than 1×10^{-4} according to the nearly stable modulus of granite at higher pressures (deep depth). A high amount of accumulated strain generates large shear stress and the contribution of 1×10^{-4} strain to horizontal stress is estimated at 10 MPa (with a modulus of 100 GPa). Simultaneously, if the strain increase is caused by continuous deformation, considering a strain variation of 10^{-7} per year (Wang and Shen, 2020), the increase in strain by a magnitude of 1×10^{-4} requires approximately 1,000 years. Given the stress drop and earthquake recurrence interval, a strain of 1×10^{-4} is equivalent to the strain consumed by several earthquakes with magnitude larger than 5.0 (Allmann and Shearer, 2009; Li and Shibazaki, 2014). A similar seismic activity should be observed among these three faults according to the elastic storage energy. However, the seismicity of the Anninghe Fault is much lower than those of the other two faults. One of the reasons may be their different geothermal gradients that influence the mechanical behaviors in their deep parts. The high geothermal gradients in the Anninghe Fault (Wang et al., 2018) expands the low-stress layer in the upper crust near the UL boundary, exhibiting the easy condition for aseismic slip (Xu and Zeng, 2022). Hence, the Anninghe Fault is similar to a deformation channel by the slip of fault (Zhang, 2008), where low-stress layer exists from the upper crust, generating a decoupled upper and lower crust and leading to a low seismicity. In the Xianshuihe Fault, the low-stress layer in the upper crust is only partial distributed and stress can still accumulate in the upper and lower crust, resulting in relatively high seismicity. The low geothermal gradient in the Longmenshan Fault prevents the generation of low-stress layer in 16–18 km depth of the upper crust. Therefore, the strong upper and lower crust below the Longmenshan Fault makes it difficult for slip occurring and earthquakes with long recurrence interval and large magnitude generate easily. This finding is similar to the results of the strain rate from GPS inversion, that is, a dilatation state is observed in the west of the Anninghe Fault and a contraction state is recorded in the Longmenshan and Xianshuihe Faults (Wang and Shen, 2020). Furthermore, in the Anninghe Fault, a seismic gap appears at a depth around 8 km (Figure 5). However, determining whether it is seismic gap is difficult because of the small

number of seismic events, and the stress model cannot display this low-stress layer due to present data. Although the mechanism of seismogenesis is controlled by many other factors, the depth of the lower crust combined with the geothermal gradient plays a vital role in determining the stress distribution and understanding the mechanism of earthquake genesis. Finally, the present results mainly exhibit the overall stress differences between these three faults. The resolution of the geothermal gradients used in this study is at a scale of approximately 10 km. The details in some sections of these three faults may not display very well, especially for the southeast section of Xianshuihe Fault, which shows complexity of velocity, geothermal gradient, and stress environment (Li et al., 2015; 2023; Liu et al., 2023; 2017; Liang et al., 2023; Sun et al., 2023; Sun et al., 2021; Cheng et al., 2022; Zhu et al., 2024). More detailed works are needed in the future for stress investigation on the local sections of these three faults.

4.3 Implications in general continental crust

In this paper, our results are obtained in the area of the SETP, but they also provide insights for studying multiple processes (such as crustal deformation, fault slip, and earthquake occurrence) in the continental crust around the world. First, our model demonstrates a new method to investigate the detailed stress distribution in the continental crust. Our approach calculates the detailed stress distribution at different depths and explains multiple observations from geophysics, geology, and laboratory. Second, our results clearly demonstrate the relationships between differential stress, brittle–ductile transition, seismicity, and UL boundary. The decrease in differential stress corresponds to the brittle–ductile transition, which is caused by rheological deformation due to temperature. The brittle–ductile transition causes the decrease in seismicity. Though the brittle–ductile transition occurs near the UL boundary, they are caused by different mechanisms. The UL boundary cannot be determined by the decrease in seismicity. The increase in pyroxenes or feldspar at the UL boundary causes the increase in differential stress. Therefore, the brittle–ductile transition can cause low seismicity due to dissipation of differential stress, whereas the UL boundary may cause the increase in seismicity due to the increase in differential stress. Different areas show distinct characteristics in depth distribution of earthquakes (Maggi et al., 2000). Our findings can help further understand the stress environment of the seismogenic zone in the continental crust around the world, such as the North America (Mogistrale, 2002), the Central and East Asia (Sloan et al., 2011; Dong et al., 2018), and the East African (Albaric et al., 2009; Craig et al., 2011).

5 Conclusion

The crustal stress model with different depths (15, 20, and 25 km) of the UL boundary below the Anninghe, Xianshuihe, and Longmenshan Faults in the SETP are built based on *in situ* stress data and rock rheological properties. The results suggest that the 20 km depth of the UL boundary and the different geothermal gradients in the SETP can account for most geophysical and geological observations, such as composition, *in situ* stress, electric conductivity, and velocity structures. The differential stress distribution against depth reveals a different type of brittle–ductile transition (double-layer) below the Anninghe Fault from that (single-layer) below the Longmenshan Fault, whereas it shows both types below the Xianshuihe Fault, agreeing with their focal depth distributions. This observation can be explained by geothermal gradient differences among these three faults. The stress model provides new insights for understanding the stress environment of the seismogenic zone in the SETP. The relatively wider low-stress layer in the bottom of the upper crust easily dissipates the stress to prevent the generation of large earthquakes in the Anninghe Fault compared with that in the Xianshuihe Fault, whereas the low-stress layer only appears in the lower crust below the Longmenshan Fault, suggesting a special upper crust that facilitates stress accumulation. Our model further clarifies the relationships between differential stress, seismicity, brittle–ductile transition, and boundary depth of the upper and lower continental crust. By combining with geothermal gradients, the composition variation between the upper and lower crust can strongly cause the change of differential stress, thereby affecting the brittle–ductile transition and depth distribution of earthquakes. Furthermore, our results demonstrate that multiple observations from geophysics, geology, and laboratory can verify one another and provide a more detailed understanding for the environment of the seismogenic zone in the continental crust.

Data availability statement

The raw data supporting the conclusions of this article will be made available by the authors, without undue reservation.

Author contributions

JX: Data curation, Formal Analysis, Funding acquisition, Methodology, Writing–original draft, Writing–review and editing. XZ: Funding acquisition, Writing–original draft, Writing–review and editing.

Funding

The author(s) declare that financial support was received for the research, authorship, and/or publication of this article. This work was supported by the National Natural Science Foundation of China (Grant No. U2239203 and 41941016).

Acknowledgments

The authors would like to thank Dr. Jianxin Wang for part of *in-situ* stress data and Dr. Jian Wang for the geothermal data. This manuscript was much improved by thoughtful reviews of Prof. Valerio Acocella and four reviewers.

Conflict of interest

The authors declare that the research was conducted in the absence of any commercial or financial relationships that could be construed as a potential conflict of interest.

Publisher's note

All claims expressed in this article are solely those of the authors and do not necessarily represent those of their affiliated organizations, or those of the publisher, the editors and the reviewers. Any product that may be evaluated in this article, or claim that may be made by its manufacturer, is not guaranteed or endorsed by the publisher.

Supplementary material

The Supplementary Material for this article can be found online at: https://www.frontiersin.org/articles/10.3389/feart.2024.1439493/full#supplementary-material

References

Aki, K., and Richards, P. G. (1980). *Quantitative seismology-theory and methods*. San Francisco: W.H. Freeman and Company.

Albaric, J., Déverchère, J., Petit, C., Perrot, J., and Gall, B. L. (2009). Crustal rheology and depth distribution of earthquakes: insights from the central and southern East African Rift System. *Tectonophysics* 468, 28–41. doi:10.1016/j.tecto.2008.05.021

Allmann, B. P., and Shearer, P. M. (2009). Global variations of stress drop for moderate to large earthquakes. *J. Geophys. Res. Solid Earth* 114, B01310. doi:10.1029/2008JB005821

An, Z., Kutzbach, J. E., Prell, W. L., and Porter, S. C. (2001). Evolution of Asian monsoons and phased uplift of the Himalaya–Tibetan plateau since Late Miocene times. *Nature* 411, 62–66. doi:10.1038/35075035

Bao, X., Sun, X., Xu, M., Eaton, D. W., Song, X., Wang, L., et al. (2015). Two crustal low-velocity channels beneath SE Tibet revealed by joint inversion of Rayleigh wave dispersion and receiver functions. *Earth Planet. Sci. Lett.* 415, 16–24. doi:10.1016/j.epsl.2015.01.020

Blake, O. O., Faulkner, D. R., and Tatham, D. J. (2019). The role of fractures, effective pressure and loading on the difference between the static and dynamic Poisson's ratio and Young's modulus of Westerly granite. *Int. J. Rock Mech. Min. Sci.* 116, 87–98. doi:10.1016/j.ijrmms.2019.03.001

Blanton, T. L., and Olson, J. E. (1999). Stress magnitudes from logs: effects of tectonic strains and temperature. *SPE Reserv. Eval. and Eng.* 2, 62–68. doi:10.2118/54653-pa

Brown, E. T., and Hoek, E. (1978). Trends in relationships between measured *in-situ* stresses and depth. *Int. J. Rock Mech. Min. Sci. and Geomechanics Abstr.* 15, 211–215. doi:10.1016/0148-9062(78)91227-5

Bürgmann, R., and Dresen, G. (2008). Rheology of the lower crust and upper mantle: evidence from rock mechanics, geodesy, and field observations. *Annu. Rev. Earth Planet. Sci.* 36, 531–567. doi:10.1146/annurev.earth.36.031207.124326

Byerlee, J. (1978). Friction of rocks. *Pure Appl. Geophys.* 116, 615–626. doi:10.1007/BF00876528

Chen, J., Jin, Z., Liu, W., Wang, Y., and Zhang, J. (2021). Rheology of dry K-feldspar aggregates at high temperature and high pressure: an experimental study. *Tectonophysics* 817, 229072. doi:10.1016/j.tecto.2021.229072

Chen, Q., Feng, C., Meng, W., Qin, X., and An, Q. (2012). Analysis of *in situ* stress measurements at the northeastern section of the Longmenshan fault zone after the 5.12 Wenchuan earthquake. *Chin. J. Geophys. Chin. Ed.* 55, 3923–3932. doi:10.6038/j.issn.0001-5733.2012.12.005

Cheng, Y., Pang, Z., Kong, Y., Chen, X., and Wang, J. (2022). Imaging the heat source of the kangding high-temperature geothermal system on the Xianshuihe fault by magnetotelluric survey. *Geotermics* 102, 102386. doi:10.1016/j.geothermics.2022.102386

Clark, M. K., and Royden, L. H. (2000). Topographic ooze: building the eastern margin of Tibet by lower crustal flow. *Geology* 28, 703–706. doi:10.1130/0091-7613(2000)028<0703:tobtem>2.3.co;2

Craig, T. J., Jackson, J. A., Priestley, K., and McKenzie, D. (2011). Earthquake distribution patterns in Africa: their relationship to variations in lithospheric and geological structure, and their rheological implications. *Geophys. J. Int.* 185, 403–434. doi:10.1111/j.1365-246X.2011.04950.x

Dong, Y., Ni, S., Yuen, D. A., and Li, Z. (2018). Crustal rheology from focal depths in the North China Basin. *Earth Planet. Sci. Lett.* 497, 123–138. doi:10.1016/j.epsl.2018.06.018

Fairhurst, C. (2003). Stress estimation in rock: a brief history and review. *Intern. J. Rock Mech. Min. Sci.* 40, 957–973. doi:10.1016/j.ijrmms.2003.07.002

Fukuda, J., Muto, J., Koizumi, S., Sawa, S., and Nagahama, H. (2022). Enhancement of ductile deformation in polycrystalline anorthite due to the addition of water. *J. Struct. Geol.* 156, 104547. doi:10.1016/j.jsg.2022.104547

Gleason, G. C., and Tullis, J. (1995). A flow law for dislocation creep of quartz aggregates determined with the molten salt cell. *Tectonophysics.* 247, 1–23. doi:10.1016/0040-1951(95)00011-B

Hacker, B. R., Kelemen, P. B., and Behn, M. D. (2015). Continental lower crust. *Annu. Rev. Earth Planet. Sci.* 43, 167–205. doi:10.1146/annurev-earth-050212-124117

Haimson, B. C. (1978). The hydrofracturing stress measuring method and recent field results. *Int. J. Rock Mech. Min. Sci. and Geomechanics Abstr.* 15, 167–178. doi:10.1016/0148-9062(78)91223-8

Hanks, T. C., and Raleigh, C. B. (1980). The conference on magnitude of deviatoric stresses in the Earth's crust and uppermost mantle. *J. Geophys. Res. Solid Earth* 85, 6083–6085. doi:10.1029/JB085iB11p06083

Heidbach, O., Rajabi, M., Reiter, K., and Ziegler, M. (2019). "World stress map," in *In Encyclopedia of petroleum geoscience* (Germany: Springer), 1–8.

Hu, J., Xu, X., Yang, H., Wen, L., and Li, G. (2011). S receiver function analysis of the crustal and lithospheric structures beneath eastern Tibet. *Earth Planet. Sci. Lett.* 306, 77–85. doi:10.1016/j.epsl.2011.03.034

Huang, R., Wang, Z., Pei, S., and Wang, Y. (2009). Crustal ductile flow and its contribution to tectonic stress in Southwest China. *Tectonophysics* 473, 476–489. doi:10.1016/j.tecto.2009.04.001

Hubbert, M. K., and Rubey, W. W. (1959). Role of fluid pressure in mechanics of overthrust faulting: I. Mechanics of fluid-filled porous solids and its application to overthrust faulting. *GSA Bull.* 70, 115–166. doi:10.1130/0016-7606(1959)70[115:ROFPIM]2.0

Jackson, J. A. (2002). Faulting, flow, and strength of the continental lithosphere. *Int. Geol. Rev.* 11, 39–61. doi:10.2747/0020-6814.44.1.39

Ji, S., and Zhao, P. (1993). Flow laws of multiphase rocks calculated from experimental data on the constituent phases. *Earth Planet. Sci. Lett.* 117, 181–187. doi:10.1016/0012-821X(93)90125-S

Laske, G., Masters, G., Ma, Z., and Pasyanos, M. E. (2013). Update on CRUST1.0 - a 1-degree global model of earth's crust. *Geophys. Res. Abstr.* 15, EGU2013–2658.

Li, B., Xie, F., Huang, J., Xu, X., Guo, Q., Zhang, G., et al. (2022). *In situ* stress state and seismic hazard in the Dayi seismic gap of the Longmenshan thrust belt. *Sci. China Earth Sci.* 65, 1388–1398. doi:10.1007/s11430-021-9915-4

Li, C. F., Wang, J., Lin, J., and Wang, T. (2017). Thermal evolution of the North Atlantic lithosphere: new constraints from magnetic anomaly inversion with a fractal magnetization model. *Geochem. Geophys. Geosystems* 14, 5078–5105. doi:10.1002/2013GC004896

Li, D., Ding, Z., Wu, P., Zheng, C., Ye, Q., and Liang, M. (2015). The deep seismogenic environment of the southeastern section of the Xianshuihe fault zone and the 2014 Kangding *Ms* 6.3 earthquake. *Chin. J. Geophys. Chin. Ed.* 58, 1941–1953. doi:10.6038/cjg20150610

Li, X., and Shibazaki, B. (2014). 3D modeling of earthquake cycles of the Xianshuihe fault, southwestern China. *J. Asian Earth Sci.* 96, 205–212. doi:10.1016/j.jseaes.2014.08.040

Li, Y., Liu, M., Li, Y., and Chen, L. (2019). Active crustal deformation in southeastern Tibetan plateau: the kinematics and dynamics. *Earth Planet. Sci. Lett.* 523, 115708. doi:10.1016/j.epsl.2019.07.010

Li, Y., Tian, J., Li, X., Li, S., Wang, Q., and Gao, Y. (2023). Deep tectonic pattern of the luding *ms* 6.8 earthquake on 5th september 2022 in sichuan province, China. *Chin. J. Geophys. Chin. Ed.* 66, 1385–1396. doi:10.6038/cjg2023Q0742

Liang, J., Yu, Y., Shi, Z., Li, Z., Huang, Y., Song, H., et al. (2023). Geothermal springs with high δ13CCO2-DIC along the Xianshuihe fault, Western Sichuan, China: a geochemical signature of enhanced deep tectonic activity. *J. Hydrology* 623, 129760. doi:10.1016/j.jhydrol.2023.129760

Liu, Q., Shi, Y., Wei, D., Han, P., Chen, S., Liu, P., et al. (2017). Near-surface geothermal gradient observation and geothermal analyses in the Xianshuihe fault zone, eastern Tibetan Plateau. *Acta Geol. Sinica-English Ed.* 91, 414–428. doi:10.1111/1755-6724.13108

Liu, Y., Yu, Z., Zhang, Z., Yao, H., Wang, W., Zhang, H., et al. (2023). The high-resolution community velocity model V2.0 of southwest China, constructed by joint body and surface wave tomography of data recorded at temporary dense arrays. *Sci. China Earth Sci.* 66, 2368–2385. doi:10.1007/s11430-022-1161-7

Maggi, A., Jackson, J. A., McKenzie, D., and Priestley, K. (2000). Earthquake focal depths, effective elastic thickness, and the strength of the continental lithosphere. *Geology* 28, 495–498. doi:10.1130/0091-7613(2000)028<0495:efdeet>2.3.co;2

Masuti, S., Muto, J., and Rybacki, E. (2023). Transient creep of quartz and granulite at high temperature under wet conditions. *J. Geophys. Res. Solid Earth* 128, e2023JB027762. doi:10.1029/2023JB027762

Meade, B. J. (2007). Present-day kinematics at the India-Asia collision zone. *Geology* 35, 81–84. doi:10.1130/G22924A.1

Mogistrale, H. (2002). Relative contributions of crustal temperature and composition to controlling the depth of earthquakes in Southern California. *Geophys. Res. Lett.* 29, 87. doi:10.1029/2001GL014375

Nur, A., and Simmons, G. (1969). The effect of saturation on velocity in low porosity rocks. *Earth Planet. Sci. Lett.* 7, 183–193. doi:10.1016/0012-821X(69)90035-1

Ren, Y., Wang, D., Li, T., Ran, X., Liu, Z., and Zhang, J. (2021). *In-situ* geostress characteristics and engineering effect in Ya'an-Xinduqiao section of Sichuan-Tibet Railway. *Chin. J. Rock Mech. Eng.* 40, 65–76. doi:10.13722/j.cnki.jrme.2020.0537

Royden, L. H., Burchfiel, B. C., King, R. W., Wang, E., Chen, Z. L., Shen, F., et al. (1997). Surface deformation and lower crustal flow in eastern Tibet. *Science* 276, 788–790. doi:10.1126/science.276.5313.788

Royden, L. H., Burchfiel, B. C., and van der Hilst, R. D. (2008). The geological evolution of the Tibetan Plateau. *Science* 321, 1054–1058. doi:10.1126/science.1155371

Rudnick, R. L., and Gao, S. (2003). Composition of the continental crust. *Treatise Geochem. 2nd Ed.* 3, 1–64. doi:10.1016/B0-08-043751-6/03016-4

Rutter, E. H., Brodie, K. H., and Irving, D. H. (2006). Flow of synthetic, wet, partially molten "granite" under undrained conditions: an experimental study. *J. Geophys. Res. Solid Earth* 111, B06407. doi:10.1029/2005JB004257

Rybacki, E., and Dresen, G. (2000). Dislocation and diffusion creep of synthetic anorthite aggregates. *J. Geophys. Res. Solid Earth* 105, 26017–26036. doi:10.1029/2000JB900223

Savage, W. Z., Swolfs, H. S., and Amadei, B. (1992). On the state of stress in the near-surface of the Earth's crust. *Pure Appl. Geophys.* 138, 207–228. doi:10.1007/BF00878896

Scholz, C. H. (2002). *The mechanics of earthquakes and faulting*. Cambridge: Cambridge University Press.

Sen, Z., and Sadagah, B. H. (2002). Probabilistic horizontal stress ratios in rock. *Math. Geol.* 34, 845–855. doi:10.1023/A:1020928727867

Sheorey, P. R. (1994). A theory for *in situ* stresses in isotropic and transverseley isotropic rock. *Intern. J. Rock Mech. Min. Sci. and Geomechanics Abstr.* 31, 23–34. doi:10.1016/0148-9062(94)92312-4

Sloan, R. A., Jackson, J. A., McKenzie, D., and Priestley, K. (2011). Earthquake depth distributions in central Asia, and their relations with lithosphere thickness, shortening and extension. *Geophys. J. Int.* 185, 1–29. doi:10.1111/j.1365-246X.2010.04882.x

Sun, L., Zhao, Z., Pan, J., Liang, F., Zhang, L., and Zhang, J. (2021). The stress and strain state of Yalahe fault in the Kangding segment of the Xianshuihe fault zone and its seismogenic environment. *Acta Petrol. Sin.* 37, 3225–3240. doi:10.18654/1000-0569/2021.10.15

Sun, Y., Li, H., Fan, T., and Li, B. (2023). Effect of rheological heterogeneities on the lithospheric deformation of the Tibetan Plateau and neighbouring regions. *Front. Earth Sci.* 11, 1153744. doi:10.3389/feart.2023.1153744

Tanaka, A., Okubo, Y., and Matsubayashi, O. (1999). Curie point depth based on spectrum analysis of the magnetic anomaly data in East and Southeast Asia. *Tectonophysics* 306, 461–470. doi:10.1016/S0040-1951(99)00072-4

Tapponnier, P., Xu, Z. Q., Roger, F., Meyer, B., Arnaud, N., Wittlinger, G., et al. (2001). Oblique stepwise rise and growth of the Tibet Plateau. *Science* 294, 1671–1677. doi:10.1126/science.105978

Tian, J., Pang, Z., Liao, D., and Zhou, X. (2021). Fluid geochemistry and its implications on the role of deep faults in the genesis of high temperature systems in the eastern edge of the Qinghai Tibet Plateau. *Appl. Geochem.* 131, 105036. doi:10.1016/j.apgeochem.2021.105036

Tullis, T. E., Horowitz, F. G., and Tullis, J. (1991). Flow laws of polyphase aggregates from end-member flow laws. *J. Geophys. Res. Solid Earth* 96, 8081–8096. doi:10.1029/90JB02491

Ullah, J., Luo, M., Ashraf, U., Pan, H., Anees, A., Li, D., et al. (2022). Evaluation of the geothermal parameters to decipher the thermal structure of the upper crust of the Longmenshan fault zone derived from borehole data. *Geothermics* 98, 102268. doi:10.1016/j.geothermics.2021.102268

Wan, Z. S., Zhao, G. Z., Tang, J., Chen, X. B., Wang, L. F., Xiao, Q. B., et al. (2010). The electrical structure of the crust along Mianning-Yibin profile in the eastern edge of Tibetan plateau and its tectonic implications. *Chin. J. Geophys. Chin. Ed.* 53, 585–594. doi:10.3969/j.issn.0001-5733.2010.03.012

Wang, C., Han, W., Wu, J., Lou, H., and Chan, W. W. (2007). Crustal structure beneath the eastern margin of the Tibetan Plateau and its tectonic implications. *J. Geophys. Res. Solid Earth* 112, B07307. doi:10.1029/2005JB003873

Wang, J., Zhang, G. W., Li, C. F., and Liang, S. S. (2018). Correlating seismicity to Curie-point depths in the eastern margin of the Tibetan Plateau. *Chin. J. Geophys. Chin. Ed.* 61, 1840–1852. doi:10.6038/cjg2018M0130

Wang, M., Shen, Z., Gan, W., Liao, H., Li, T., Ren, J., et al. (2008). GPS monitoring of temporal deformation of the Xianshuihe fault. *Sci. China Earth Sci.* 51, 1259–1266. doi:10.1007/s11430-008-0095-3

Wang, M., and Shen, Z. K. (2020). Present-day crustal deformation of continental China derived from GPS and its tectonic implications. *J. Geophys. Res. Solid Earth* 125, e2019JB018774. doi:10.1029/2019JB018774

Wang, W., Wu, J., Fang, L., Lai, G., and Cai, Y. (2017). Crustal thickness and Poisson's ratio in southwest China based on data from dense seismic arrays. *J. Geophys. Res. Solid Earth* 122, 7219–7235. doi:10.1002/2017JB013978

Xu, J., and Zeng, X. (2022). Tectonic stress redistribution induced by geothermal gradient difference: numerical modeling of stress around the Anninghe seismic gap in the southeastern Tibetan plateau. *Pure Appl. Geophys.* 179, 3713–3726. doi:10.1007/s00024-022-03162-1

Xu, X., Wen, X., Zheng, R., Ma, W., Song, F., and Yu, G. (2003). Pattern of latest tectonic motion and its dynamics for active blocks in Sichuan-Yunnan region, China. *Sci. China Earth Sci.* 46, 210–226. doi:10.1360/03dz0017

Yang, S., Yao, R., Cui, X., Chen, Q., and Huang, L. (2012). Analysis of the characteristics of measured stress in Chinese mainland and its active blocks and North–South seismic belt. *Chin. J. Geophys. Chin. Ed.* 55, 4207–4217. doi:10.6038/j.issn.0001–5733.2012.12.032

Yang, Y., Zhang, X., Hua, Q., Su, L., Feng, C., Qiu, Y., et al. (2021). Segmentation characteristics of the Longmenshan fault–Constrained from dense focal mechanism data. *Chin. J. Geophys. Chin. Ed.* 64, 1181–1205. doi:10.6038/cjg2021O0286

Zang, A., and Stephansson, O. (2010). *Stress field of the Earth's crust*. London: Springer.

Zhang, P. Z. (2008). Present-day tectonic deformation, strain partitioning and deep dynamics in the western Sichuan, eastern Tibetan Plateau. *Sci. China Earch Sci.* 38, 1041–1056. doi:10.1360/zd2008-38-9-1041

Zhao, G., Chen, X., Wang, L., Wang, J., Tang, J., Wan, Z., et al. (2008). Evidence of crustal 'channel flow' in eastern margin of Tibet plateau from MT measurements. *Chin. Sci. Bullettin* 52, 1887–1893. doi:10.1360/csb2008-53-3-345

Zhou, Y., Zhang, H., Yao, W., Dang, J., and He, C. (2017). An experimental study on creep of partially molten granulite under high temperature and wet conditions. *J. Asian Earth Sci.* 139, 15–29. doi:10.1016/j.jseaes.2016.10.011

Zhu, Y., Diao, F., Chen, F., Wang, Y., Shao, Z., Wang, R., et al. (2024). Probing the interseismic locking state of the Xianshuihe fault based on a viscoelastic deformation model. *Sci. China Earth Sci.* 67, 134–145. doi:10.1007/s11430-022-1152-2

Zoback, M. D., Barton, C. A., Brudy, M., Castillo, D. A., Finkbeiner, T., Grollimund, B. R., et al. (2003). Determination of stress orientation and magnitude in deep wells. *Int. J. Rock Mech. Min. Sci.* 40, 1049–1076. doi:10.1016/j.ijrmms.2003.07.001

Zoback, M. D., and Townend, J. (2001). Implications of hydrostatic pore pressures and high crustal strength for the deformation of intraplate lithosphere. *Tectonophysics* 336, 19–30. doi:10.1016/S0040-1951(01)00091-9

Zoback, M. L. (1992). First-and second-order patterns of stress in the lithosphere: the world stress map project. *J. Geophys. Res. Solid Earth* 97, 11703–11728. doi:10.1029/92JB00132